ISTANBUL TECHNICAL UNIVERSITY ★ FACULTY OF AERONAUTICS AND ASTRONAUTICS

CFD ANALYSIS OF A BLUNT BODY FOR MARS ENTRY

GRADUATION PROJECT

ERDİNÇ YAKUT

Department of Astronautical Engineering

Thesis Advisor: Assist. Prof. Dr. Bayram ÇELİK

AUGUST 2014

ISTANBUL TECHNICAL UNIVERSITY ★ FACULTY OF AERONAUTICS AND ASTRONAUTICS

CFD ANALYSIS OF A BLUNT BODY FOR MARS ENTRY

GRADUATION PROJECT

Erdinç YAKUT

110090101

Department of Astronautical Engineering

Thesis Advisor: Assist. Prof. Dr. Bayram ÇELİK

AUGUST 2014

Erdinç YAKUT, student of ITU Faculty of Aeronautics and Astronautics student ID 110090101, successfully defended the **graduation** entitled "**CFD Analysis of a Blunt Body for Mars Entry"** which he prepared after fulfilling the requirements specified in the associated legislations, before the jury whose signatures are below.

Thesis Advisor: Assist. Prof. Dr. Bayram ÇELİK .....

Jury Members: Assist. Prof. Dr. K. Bülent YÜCEİL .....

Dr. Bülent TUTKUN .....

Date of Submission: 22 August2014

Date of Defense: 21 August 2014

To My Family;

Nermin, Nevzat & Dinçer YAKUT

FOREWORD

First and foremost, I sincerely would like to thank my thesis advisor Assist. Prof. Dr. Bayram Çelik for supporting and guiding me in this thesis.

Secondly, I especially would like to thank Gümüş Aerospace & Defense Ltd. and Metacomp Technology, Inc. for their supporting and giving a chance for studying atmospheric entry by using CFD++ software. In addition, I would like to thank Murat Süer for his support and encouragement always to do better through my university life.

Thirdly, my friends, Aykut Özbeytemur, Cem Oran and Eray Koç for their contribution to my life with their precious ideas.

Eventually, I would like to thank and express my gratitude to my mother, Nermin Yakut, my father, Nevzat Yakut, and my brother, Dinçer Yakut without them i would not be the same person i am right now.

August 2014 Erdinç YAKUT

TABLE OF CONTENTS

NOTATIONS

Kn : Knudsen Number

DSMC : Direct Simulation Monte Carlo

CFD : Computational Fluid Dynamics

DLR : German Aerospace Center

Q : Dependent Variable Vector

$\mathbf{F_i}$: Inviscid Flux Vectors

$\mathbf{G_i}$: Viscous Flux Vectors

$\dot{S}$: Source Term Vector

E : Total Energy

P : Pressure

u : x-Direction Velocity

v : y-Direction Velocity

ω : z-Direction Velocity

σ_i : Mass Fraction of Species i

D : Diffusivity Constant

ω_{ik} : Mass Rate Per Unit Volume of Production of i from reaction k

$\bar{\mu}_m$: Laminar Viscosity of the Mixture

Φ : Dilation

$\bar{k}_m$: Thermal Conductivity of the Mixture

ν'_{ik} : Stoichiometric Coefficient of i in reactant side of step k

ν''_{ik} : Stoichiometric Coefficient of i in product side of step k

M_i : Chemical Symbol of i

K_{fk} : Forward Rate Constant for Reaction k

K_{bk} : Backward Rate Constant for Reaction k

$\mathbf{N_P}$: Exponent of Pressure in the Rate Constant of Reaction k

N_T : Exponent of Temperature in the Rate Constant of Reaction k

R_0 : Universal Gas Constant

T : Static Temperature

$\overline{W_i}$: Molecular Weight of i

C_l : Molar Concentration of Species i

$\overline{A_k}$: Preexponential Factor for Reaction Step k

E_{Ak} : Activation Energy of Reaction Step k

g_i : Gibbs Free Energy of i

TABLE LIST

Page Number

FIGURE LIST

Page Number

CFD ANALYSIS OF A BLUNT BODY FOR MARS ENTRY

SUMMARY

In this study, hypersonic flowfield around a blunt body is investigated by using a commercial computational fluid dynamic (CFD) package program, CFD++. CFD++ is a finite volume Navier-Stokes solver, which has ability of efficient simulation of both high and low speed reacting flows.

In this study, Pathfinder spacecraft has modelled and investigated as a blunt body.

First of all, a hypersonic flow example around a cylindrical blunt body, which created for CFD++ validation using data of German Aerospace Centre's (DLR) results of test case and CFD software for Mars atmosphere, is based for modelling and investigation. In this example, a cylindrical probe is at hypersonic speed. After this examination, Pathfinder spacecraft, which was launched on 4th of December 1996 and entered to atmosphere of Mars on 4th of July 1997, is modelled by using NASA's references. Its two dimensional geometry was created by using CATIA package program. After modelling the geometry, mesh of Pathfinder spacecraft's flowfield is generated via using Pointwise package program.

Finally, Pathfinder entry vehicle is examined for hypersonic flow, where the velocity and Mach number are 3257 m/s and 7.06, respectively. Variation of pressure, temperature and the concentration of the molecules and atoms in around the geometry are obtained.

KÜT BİR CİSMİN MARS'A GİRİŞİNİN HAD ANALİZLERİ

ÖZET

Bu çalışmada, küt bir cismin etrafındaki hipersonik akış, ticari bir hesaplamalı akışkanlar dinamiği (HAD) yazılımı kullanılarak incelenmiştir. Bu paket program CFD++, hesaplamalı akışkanlar dinamiği analiz yöntemini uygulamaktadır. Küt cisim geometrisi olarak, Pathfinder uzay aracı modellenmiş ve incelenmiştir.

İlk olarak, modelleme ve inceleme için, CFD++ programında, Almanya Uzay Ajansı'nın (DLR) Mars atmosferi için yaptığı test ve hesaplamalı akışkanlar dinamiği yazılımı ile elde edilmiş sonuçlarla karşılaştırmak için oluşturulmuş, silindirik küt bir cisim etrafındaki hipersonik akış örneği temel alınmıştır. İncelenen örneğin ardından, 4 Aralık 1996'da fırlatılan ve Mars'a 4 Temmuz 1997'de giriş yapan Pathfinder uzay aracının incelenebilmesi için, boyut bilgileri NASA kaynaklarından alınmış ve CATIA programı ile iki boyutlu geometrisi oluşturulmuştur. Pointwise programında ise mesh oluşturularak doğrulama örneğindeki aynı koşullar ve girdiler altında analizler tekrarlanmıştır.

Sonuç olarak, Pathfinder uzay aracı etrafındaki 3257 m/s hızında ve 7.06 Mach değerindeki hipersonik akış ile incelenmiştir. Basınç, sıcaklık ve ortamdaki molekül ve atomların dağılımları sunulmuştur.

1. INTRODUCTION

1.1 What is atmospheric entry

Humanity always want to access easily to space, but returning to Earth is an important problem. If a spacecraft needs to access to space, it must reach a specific speed because of Earth`s gravitational force. This speed is around 5 km/s. For manned missions returning to Earth is a requirement; however, after reaching to space, spacecraft has high trajectory speed. Humankind have dealt with atmospheric entries immediately after reaching space, because the key point of the planetary exploration is to enter to the target planet with handling atmospheric problems. During an atmospheric entry, the spacecraft is exposure to all regimes of the sound speed. However, the most difficult structural and environmental conditions are in hypersonic regime. Hypersonic speeds lead to high temperature, pressure, and reacting flow. It is a challenging problem for spacecraft because of the forces take place. The hypersonic speed depends on environmental conditions because of speed of sound. The equation (1.1) indicating sound speed is

$$V_{sound} = \sqrt{\gamma RT} \qquad \textbf{(1.1)}$$

γ is the ratio of specific heats, R is environmental gas constant and T is temperature. There are totally five speed regimes, namely subsonic, transonic, sonic, supersonic, and hypersonic speeds. They are classified by the ratio of gas speeds to environmental speed of sound. This ratio is called 'Mach'. Regimes of sound speeds related to Mach number are given in Table 1.1.

Table 1.1: Regimes of sound speeds.

Subsonic	Transonic	Sonic	Supersonic	Hypersonic
Mach<0.8	0.8<Mach<1.2	Mach=1	1.2<Mach<5	5<Mach

Each sound speed regimes have different properties. Commercial planes generally fly at subsonic regime. Transonic regime is not preferred because of high drag forces and instability. Supersonic regime has shocks and relatively challenging environmental conditions for crafts. Hypersonic regime has though environmental conditions. If vehicle moves in hypersonic regime, it is exposed to high temperature and pressure. Because of the high temperature levels, flow's molecules and atoms are reacting. Some molecules disassociate, ionize, and generate new atoms and molecules.

The complexity of the entry research field is caused by high speed. While a spacecraft is moving at very high speed in space, there is no important drag force on spacecraft because of space surroundings. However, if the spacecraft is wanted to land on a planet, which has an atmosphere, it is needed to reduce speed so much and land to planet surface with a small speed which is around 1 m/s. When the spacecraft is at trajectory, it has so high potential and kinetic energy because of its speed and altitude, then when it touches on the planet's surface, its kinetic energy is zero and potential energy is relatively zero. The spacecraft needs to consume this energy difference along the atmosphere. There are different way for consuming initial energy. Some of the methods of to consume energy are using retrorockets and heating the vehicle. Retrorockets are so expensive and it is impossible to use them for entry part because of fuel mass. There is a limitation to carry fuel for spacecraft because of launching and volume of spacecraft. Due to these reasons, the spacecraft needs to use heating way for entry phase. After entry phase, it can reduce speed by using supersonic parachutes and retrorockets or airbags. Landing trajectory of Pathfinder spacecraft are shown in Figure 1.1.

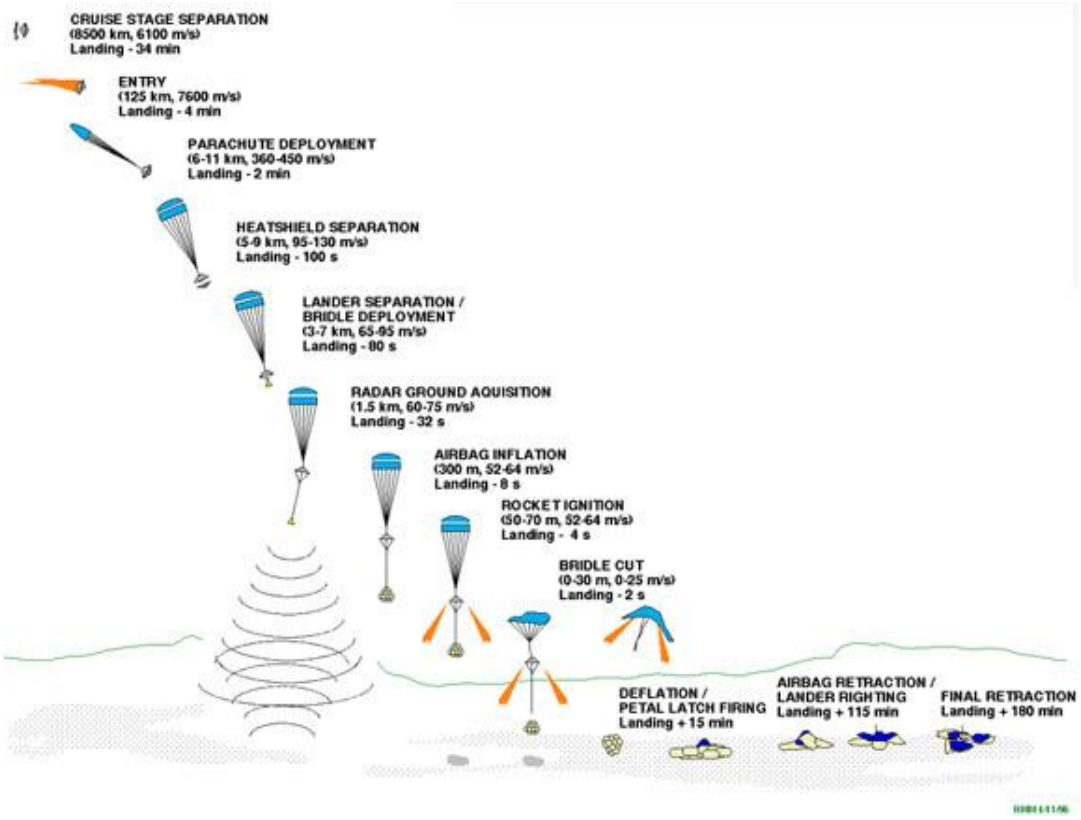

Figure 1.1: Pathfinder spacecraft atmospheric landing trajectory. [1]

In this thesis study, modelling of entry phase via CFD method is studied. The most important criteria of efficiency of an entry vehicle are reducing speed, heat and pressure. Because of reduced speed, shape of the spacecraft becomes a blunt body. Blunt bodies cause deceleration of the spacecraft. There are different blunt body types. The simplest one is cylindrical shape.

1.2 Atmospheric Entry Types

There are two main atmospheric entry types. These are controllable and uncontrollable entries. They are preferred by requirements of the missions. The uncontrollable atmospheric entry is separated two parts. These are manmade and meteoroids. Ballistic entry is a type of uncontrollable atmospheric entry. The controllable entry can be separated two parts. These are gliding and skip entries. The difference of ballistic and gliding entry are shown at Figure 1.2.

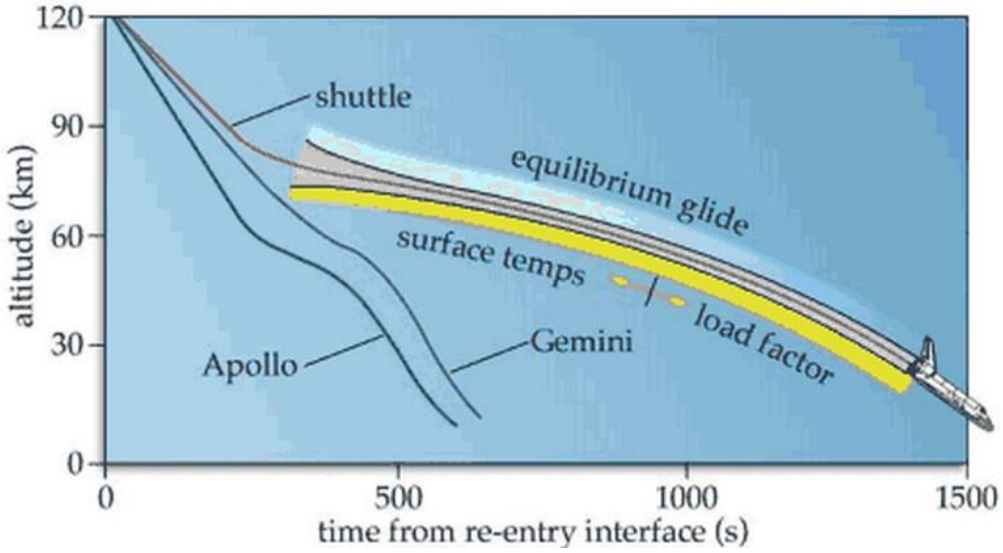

Figure 1.2: Difference of ballistic and gliding entries. [2]

1.2.1 Ballistic entry

Ballistic entry is an uncontrollable entry type, because spacecraft has only drag force to its body. Because of one force, the spacecraft cannot be controlled. Ballistic entry is based on the idea of generation of zero lift by the spacecraft. There is only drag force generated. The spacecraft that makes ballistic entry has a symmetric shape and mass distribution around one axis. It started with Mercury spacecraft for space program in 1958. The spacecraft needs to use parachutes at supersonic regimes for safely slowing down to desired speed.

1.2.2 Gliding entry

Gliding entry is a controllable entry type. An entry vehicle is able to generate lift by using unsymmetrical shape and mass distributions. If lift is able to control by vehicle, it causes good entry trajectory for reaching to the target landing area. It can use also different landing ways. One of them is flying and landing to on its wheels. This gliding entry types started with space shuttle program at 1972. The basic gliding entry types is shown in Figure 1.3.

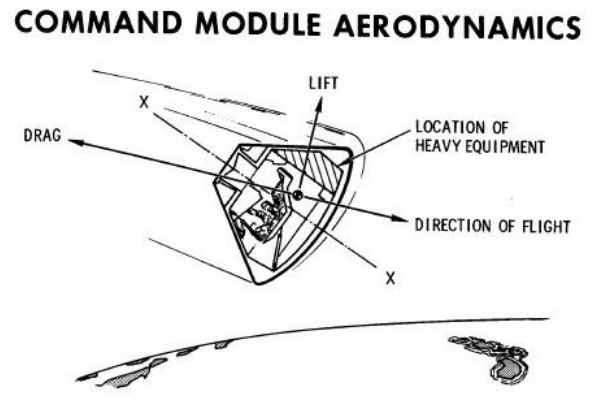

Figure 1.3: Gliding entry basic explanation. [3]

1.2.3 Skip entry

Skip entry can be a gliding or ballistic entry. The important point is before completely entering the atmosphere; spacecraft reduces speed by entering and exiting to atmosphere. The spacecraft is slowly decreasing its speed by using small drag force. It is preferred for planetary atmospheric entries because spacecrafts has high speeds at travelling interplanetary trajectories.

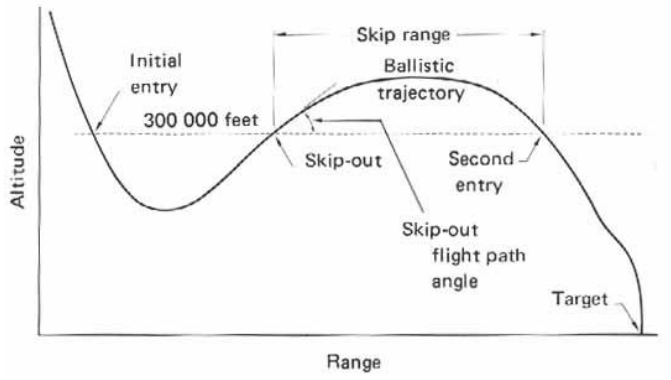

Figure 1.4: A 1963 sketch illustrating a possible skip reentry trajectory of the Apollo spacecraft. [4]

1.3 Shape of Entry Vehicles

There are many different shapes those are used vary missions. They are shown with mission names in Figure 1.5.

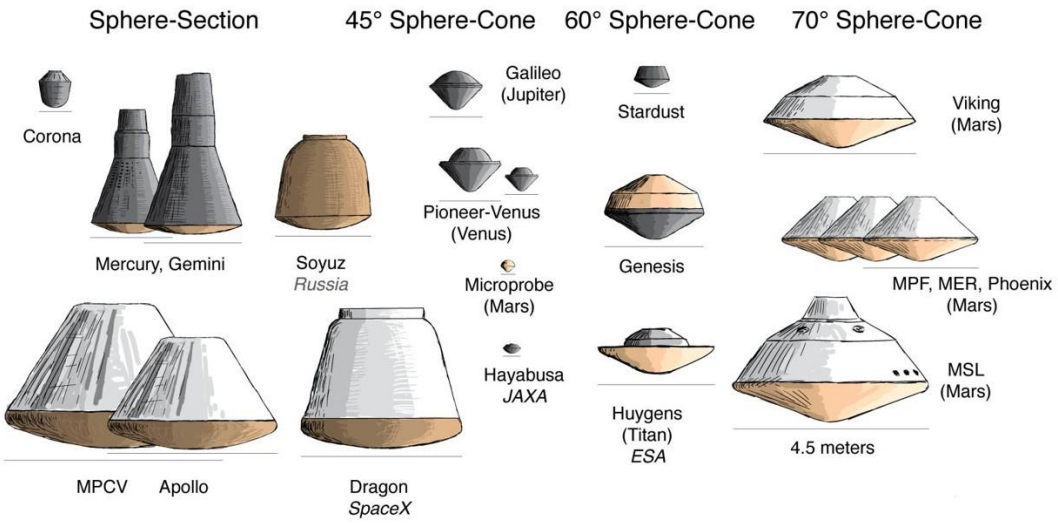

Figure 1.5: Shapes of different entry vehicles. [5]

1.4 Atmosphere Model

There are two important model for entry dynamics. These are gravity and atmosphere model. In this section, atmosphere model is considered. Atmosphere contains different molecules. The atmosphere has five different regimes depending on the altitude. These are free molecular flow, near free molecular flow, transition, viscous merged flow, continuum flow regimes. These are shown at Figure 1.6.

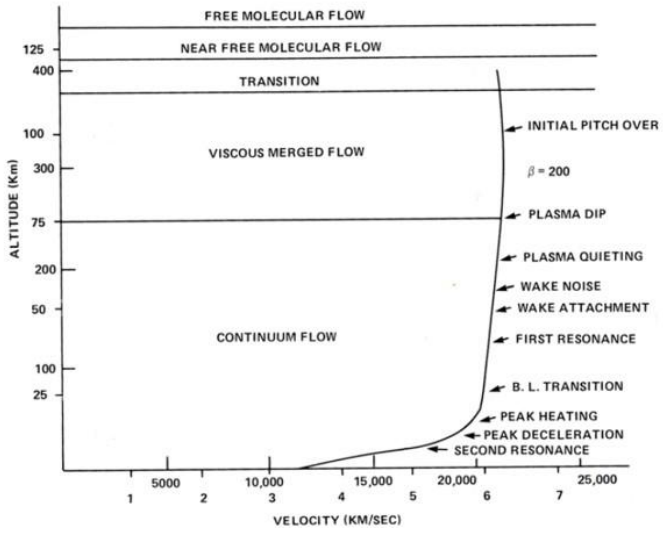

Figure 1.6: Flow regimes with typical re-entry events [6]

Because of different regimes of atmosphere, one solution procedure is not suitable for all regimes. Therefore, there are different solving technic and conditions for each

regimes. These regimes and related unique methods are shown in Figure 1.7. The Knudsen number is key parameter separating the flow regimes. The Knudsen number can be written explicitly as below. (1.2)

$$Kn = \frac{\lambda}{L} = \frac{mean\ free\ path}{characteristic\ flowfield\ dimension} \tag{1.2}$$

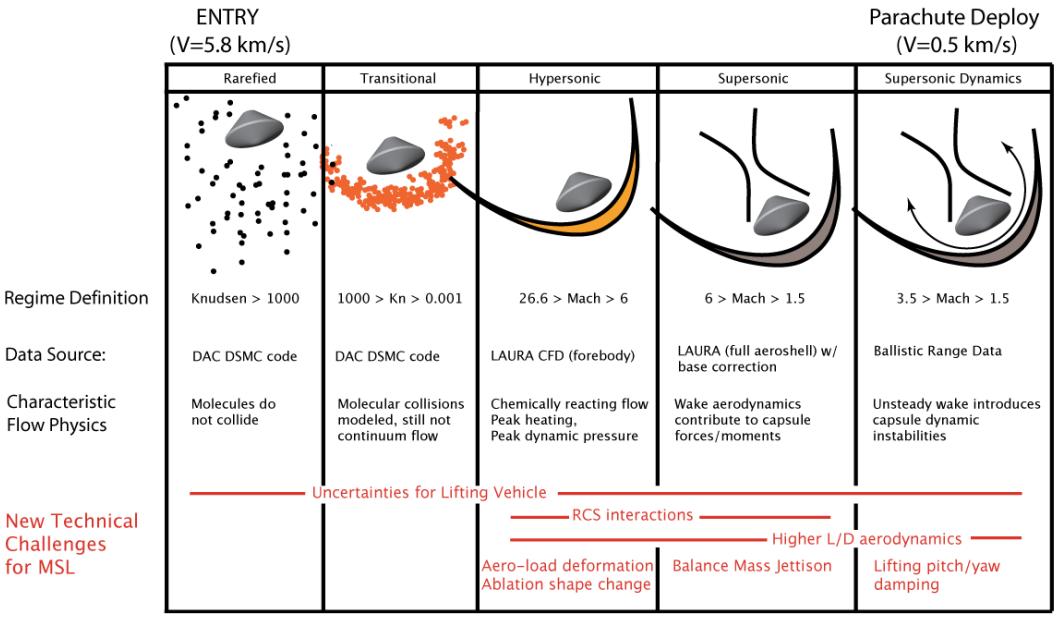

Figure 1.7: Each flight regime requires unique prediction methods. [7]

1.4.1 Free molecular flow regime

Atmospheric forces are not dominant at free molecular flow regime. Because of gravity force, the atmospheric particles are so rare. Knudsen number is higher than one. (Kn >> 1)

1.4.2 Transition flow regime

Intermolecular and molecule-surface interactions are important in the transition flow regime. The transition flow regime covers nearly free molecular flow, merged viscous region, and slip flow. In these regimes, the Navier-Stokes equations are not valid. DSMC method is able to determine around of the entry vehichle flowfield.

1.4.3 Continuum flow regime

Continuum flow regime is near the planet surface. These planets are Earth, Mars etc. In this regime, Navier-Stokes equations are able to determine the flowfield around the body. The Knudsen number is lower than 10^{-3}. (Kn << 1) Typical re-entry body flowfield is shown at Figure 1.8.

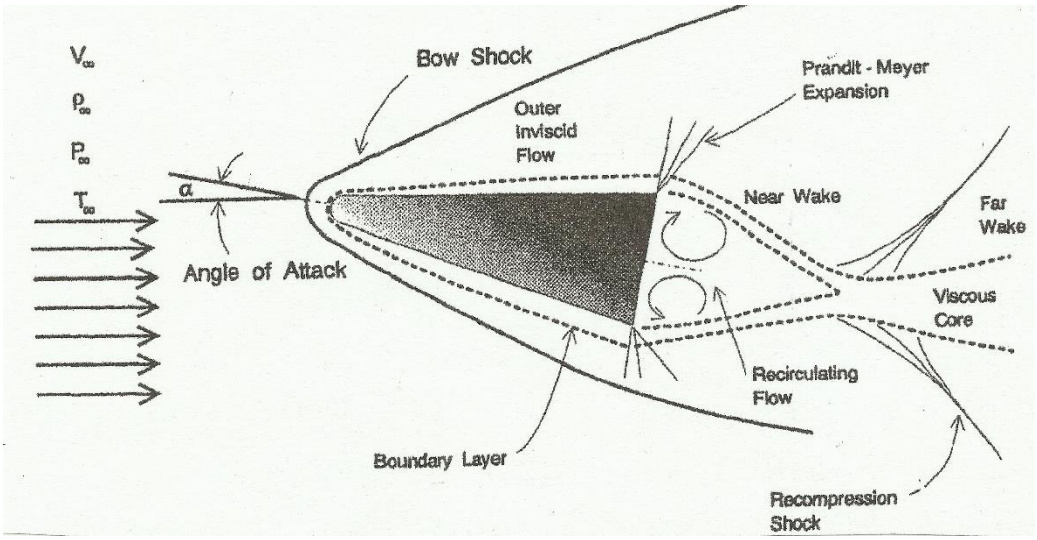

Figure 1.8: Typical re-entry body flowfield. [6]

1.5 Thesis overview

In this study, entry phenomenon is investigated and understood by tion technimodelling and solving entry problem via a CFD program. In first chapter, general information is given about solution methods for each atmosphere regimes. In second chapter, a probe example case is understood and conditions are presented. Finally, Pathfinder entry vehicle is as selected entry vehicle's geometry is drawn and its domain is meshed. Probe's conditions are applied on this case. In third chapter, results of two cases are shown. The final chapter is concludes of the thesis.

2. CFD ANALYSIS

2.1 Introduction

In this study, a commercial package program, CFD++ developed by NASA's old employers is used for understanding the solving entry problems. Two distinct problems for understanding the entry problems are solved here. First, a test case from DLR are modelled and solved. This test is described in Section 2.2. Then, the second case, Pathfinder entry vehicle is modelled and solved.

2.1.1 CFD++ and its features

CFD++ belongs to Metacomp Technologies Company. This company was founded in 1994. Metacomp Technologies is at the cutting edge of technology in Computational Fluid Dynamics (CFD), Computational Aero-Acoustics, Mesh Generation and Electrostatic Paint Deposition, with its products in widespread global use. Activities at Metacomp Technologies include research, software development, dissemination and support, consulting, education and application services.

2.2 Flow At Martian Entry Conditions around a Cylindrical Probe

This first case is from CFD++ examples. This case simulates a flow at Mars entry conditions past a blunt cylindrical probe. The probe has a diameter of 100 mm and corner radiuses of 11.5 mm. The axis of the probe is aligned with the incoming flow. This model is commonly used by the SACOMAR (Technologies for Safe and Controlled Martian Entry) project of German Aerospace Centre (DLR) to perform experimental and numerical investigations [7].

The probe's dimensions is shown in Figure 2.1. The test case probe picture is also shown in Figure 2.2.

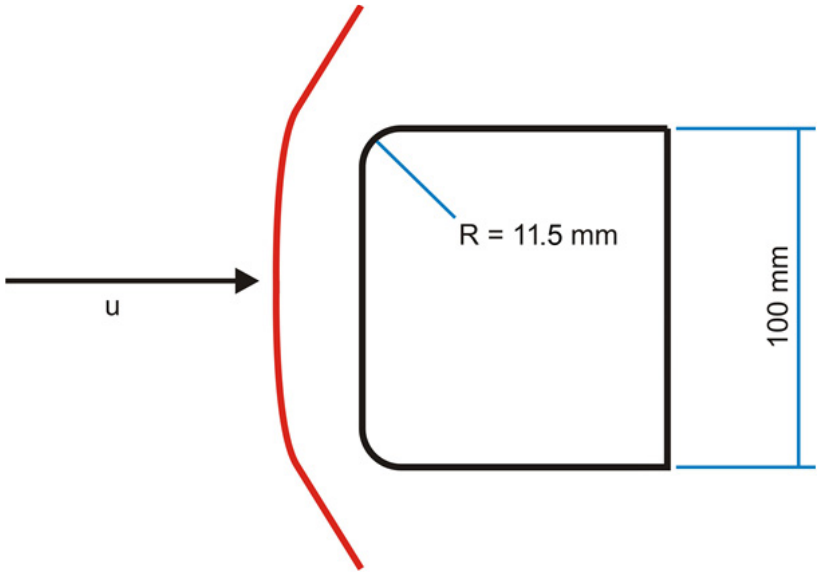

Figure 2.1: The probe case model's dimensions. [7]

Figure 2.2: Experimental probe photograph. [7]

A typical Mars entry flow condition, a pressure of 148.88 Pa, a temperature of 724 K, and a freestream of 3257 m/s are prescribed on the inflow boundary. A six species (CO_2, CO, C_2, O_2, C, O), 27 reaction model provided in [8] is employed to model chemical non-equilibrium. The flow is considered to be in thermal equilibrium. The freestream mass fractions for CO2, CO, O, and O2 are 0.562, 0.279, 0.01, and 0.149, respectively. The results from CFD++ are compared with the numerical results obtained using the DLR TAU code by Fertig [8]. These results are very compatible for pressure and temperature distributions. The comparison is shown in results section.

The default thermo-physical properties of different species in CFD++ follow the data compiled in McBride et al., 1963[9]. It covers the property variation up-to 5000 K in two temperature ranges, i.e., 100-1000 K and 1000-5000 K. For planetary entry simulations, temperatures much higher than 5000 K could be expected and therefore the species data has to be modified for such problems. For this case, CFD++ has provided data files for CO_2, CO, C_2, O_2, C and O which cover temperatures up to 15000 K in three temperature ranges, i.e., 300-1000 K, 1000-6000 K and 6000-15000 K. These files' uploading is described in CFD modelling.

2.2.1 Mesh Generation

The mesh model for case is gotten from CFD++ program examples. It has 18600 quadrilaterals mesh elements. It is shown in Figure 2.3.

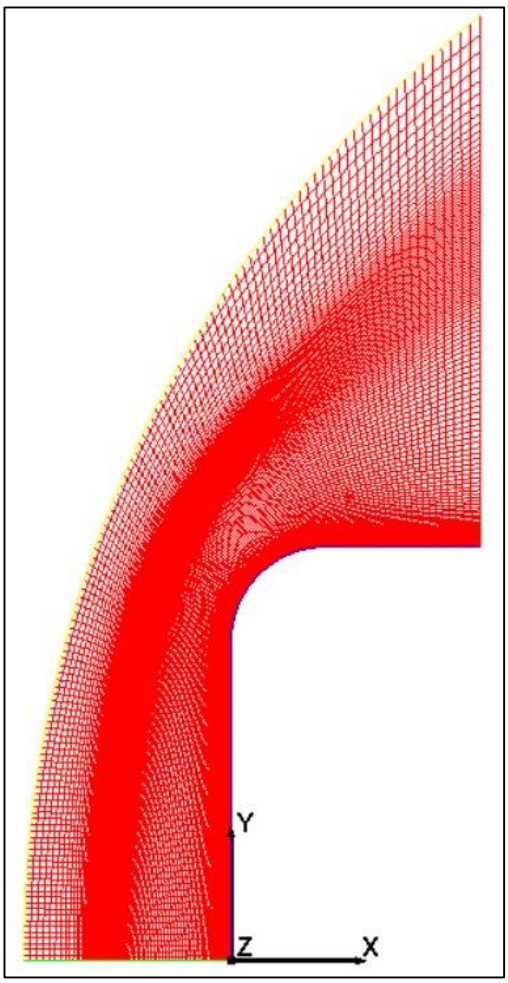

Figure 2.3: Mesh model for probe's flow field.

2.2.2 CFD modelling

Modelling a CFD case in CFD++ is so practical. Steps of case setup is indicated in following sections. In sequentially; selecting equation set type, reference quantities, fluid properties, reactions, initial conditions, boundary conditions, time integration, spatial discretization are shown in next sections.

Perfect gas assumption is not valid for entry flow because of hypersonic properties. Molecules at flow field react each other. Therefore, equation set type need to be real gas. There are some equation set type are fit for hypersonic speeds. These are compressible real gas Navier-Stokes/Euler, preconditioned/pressure-based compressible real gas Navier-Stokes/Euler, equilibrium air-Tannahill, and non-equilibrium two-temperature model. In this study, compressible real gas Navier-Stokes/Euler equation set type is preferred because of limited access to information about reactions inputs. These inputs are getting from SACOMAR test case. Although, results are agreeable with test results.

2.2.2.1 Compressible Real Gas Navier-Stokes/Euler

For a multi-species simulation, the conservation equations in two-dimensional Cartesian coordinates can be written in Equation 2.1.

$$\frac{\partial Q}{\partial t} + \frac{\partial (F_1 + G_1)}{\partial x} + \frac{\partial (F_2 + G_2)}{\partial y} + \frac{\partial (F_3 + G_3)}{\partial z} = \dot{S} \qquad \textbf{(2.1)}$$

Where Q is the dependent variable vector, F_1, F_2 and F_3 are the inviscid flux vectors; G_1, G_2 and G_3 are the viscous flux vectors; and $\dot{S}$ is the source term vector. These are given in equations 2.2, 2.3, 2.4 and 2.5.

$$Q = \begin{pmatrix} e \\ \rho \\ \rho u \\ \rho v \\ \rho \omega \\ \rho \sigma_1 \\ . \\ . \\ . \\ . \\ \rho \sigma_{N-1} \end{pmatrix} \tag{2.2}$$

$$, F_1 = \begin{pmatrix} (e+p)u \\ \rho u \\ \rho u^2 + p \\ \rho v u \\ \rho \omega u \\ \rho u \sigma_1 \\ . \\ . \\ . \\ . \\ \rho u \sigma_{N-1} \end{pmatrix}, F_2 = \begin{pmatrix} (e+p)v \\ \rho v \\ \rho u v \\ \rho v^2 + p \\ \rho \omega v \\ \rho v \sigma_1 \\ . \\ . \\ . \\ . \\ \rho v \sigma_{N-1} \end{pmatrix}, F_3 = \begin{pmatrix} (e+p)\omega \\ \rho \omega \\ \rho u \omega \\ \rho v \omega \\ \rho \omega^2 \\ \rho \omega \sigma_1 \\ . \\ . \\ . \\ . \\ \rho \omega \sigma_{N-1} \end{pmatrix} \tag{2.3}$$

$$G_1 = \begin{pmatrix} \dot{q}_x - u\tau_{xx} - v\tau_{xy} - \omega\tau_{xz} \\ 0 \\ -\tau_{xx} \\ -\tau_{xy} \\ -\tau_{xz} \\ \rho D \frac{\partial \sigma_1}{\partial x} \\ . \\ . \\ . \\ . \\ \rho D \frac{\partial \sigma_{N-1}}{\partial x} \end{pmatrix}, G_2 = \begin{pmatrix} \dot{q}_y - u\tau_{yx} - v\tau_{yy} - \omega\tau_{yz} \\ 0 \\ -\tau_{yx} \\ -\tau_{yy} \\ -\tau_{yz} \\ \rho D \frac{\partial \sigma_1}{\partial y} \\ . \\ . \\ . \\ . \\ \rho D \frac{\partial \sigma_{N-1}}{\partial y} \end{pmatrix} \tag{2.4}$$

$$G_3 = \begin{pmatrix} \dot{q}_z - u\tau_{zx} - v\tau_{zy} - \omega\tau_{zz} \\ 0 \\ -\tau_{zx} \\ -\tau_{zy} \\ -\tau_{zz} \\ \rho D \frac{\partial \sigma_1}{\partial z} \\ . \\ . \\ . \\ . \\ \rho D \frac{\partial \sigma_{N-1}}{\partial z} \end{pmatrix} \quad \textbf{(2.5)}$$

Where e is total energy, ρ is the density, p is the pressure, u, v and ω are the velocity components in the x, y and z directions respectively and σ_i is the mass fraction of species i. The species diffusion term is already written by assuming Fick's law of binary diffusion that states that all species diffuse into one another in an equal way, thus giving rise to a single diffusivity constant, D. In addition to the possible source terms arising from reactions of the form $\sum_k \omega_{ik}$ where ω_{ik} is the mass rate per unit volume of production of species i from reaction k.

For a full description of how reactions are handled in CFD++, in chemical reactions modelling section will be described.

For a Newtonian fluid, the stresses and strains are linearly related.

$$\tau_{xx} = 2\bar{\mu}_m \frac{\partial u}{\partial x} - \frac{2}{3}\bar{\mu}_m \Phi \quad \textbf{(2.6)}$$

$$\tau_{yy} = 2\bar{\mu}_m \frac{\partial v}{\partial y} - \frac{2}{3}\bar{\mu}_m \Phi \quad \textbf{(2.7)}$$

$$\tau_{zz} = 2\bar{\mu}_m \frac{\partial \omega}{\partial z} - \frac{2}{3}\bar{\mu}_m \Phi \quad \textbf{(2.8)}$$

$$\tau_{xy} = \tau_{yx} = \bar{\mu}_m(\frac{\partial u}{\partial y} + \frac{\partial v}{\partial x}) \quad \textbf{(2.9)}$$

$$\tau_{xz} = \tau_{zx} = \bar{\mu}_m\left(\frac{\partial u}{\partial z} + \frac{\partial \omega}{\partial x}\right) \quad \textbf{(2.10)}$$

$$\tau_{yz} = \tau_{zy} = \bar{\mu}_m(\frac{\partial \omega}{\partial y} + \frac{\partial v}{\partial z}) \quad \textbf{(2.11)}$$

Where $\bar{\mu}_m$ is the laminar viscosity of the mixture, and Φ is the dilation given in 2.12.

$$\Phi = \left(\frac{\partial u}{\partial x} + \frac{\partial v}{\partial y} + \frac{\partial \omega}{\partial z}\right) \quad \textbf{(2.12)}$$

From Fourier's law of conduction, these below equations can be written.

$$\dot{q}_x = -\bar{k}_m \frac{\partial T}{\partial x} \quad \textbf{(2.13)}$$

$$\dot{q}_y = -\bar{k}_m \frac{\partial T}{\partial y} \quad \textbf{(2.14)}$$

$$\dot{q}_z = -\bar{k}_m \frac{\partial T}{\partial z} \quad \textbf{(2.15)}$$

, where $\bar{k}_m$ is the thermal conductivity of the mixture.

2.2.2.2 Chemical Reactions for modelling Mars entry atmosphere

For a general chemical reaction k is need to be in equilibrium. This is described in Equation 2.16.

$$\sum_i \nu'_{ik} M_i \rightleftharpoons \sum_i \nu''_{ik} M_i \quad \textbf{(2.16)}$$

The rate of production of species i from the reaction step *k* can be written in equation 2.17.

$$\omega_{ik} = \bar{W}_i(\nu''_{ik} - \nu'_{ik})\left[K_{fk}\prod_l C_l^{\nu'_{ik}} - K_{bk}\prod_l C_l^{\nu''_{ik}}\right] \quad \textbf{(2.17)}$$

The forward rate constant for each reaction step *k* is given by Arrhenius kinetics that is shown in equation 2.18.

$$K_{fk} = \bar{A}_k T^{N_T} exp\left(\frac{-E_{Ak}}{R_0 T}\right)\left(\frac{P^{N_P}}{P_{atm}}\right) \quad \textbf{(2.18)}$$

The backward rate constant K_{bk} is computed from equilibrium condition. This equilibrium condition is shown in equation 2.19.

$$\frac{K_{fk}}{K_{bk}} = \left(\frac{P_{atm}}{R_0 T}\right)^{\sum_i(\nu''_{ik}-\nu'_{ik})} exp\left(\frac{-\Delta\bar{G}_k}{R_0 T}\right) \quad \textbf{(2.19)}$$

The change of Gibbs free energy for reaction step k is given in equation 2.20.

$$\Delta\bar{G}_k = \sum_{i=1}^{N} \nu''_{ik}\,\bar{W}_i g_i - \sum_{i=1}^{N} \nu'_{ik}\,\bar{W}_i g_i \quad \textbf{(2.20)}$$

Chemical reaction model is taken from SOCOMAR test case. It includes different 27 reactions. All reaction components are given in Table A.1 and A.2 in Appendices. Table A.1 contains reactants and products. Frequency factor, temperature exponent, and activation energy components are shown in Table A.2.

2.2.2.3 Setting initial conditions

The initial condition is taken from SACOMAR test case. These conditions are defined in Table 2.1. There are different ways in order to set up initialization. These are entire domain, cell ranges, xyz boxes, cell groups, and x-cylinder, y-cylinder, z-cylinder, and cell groups. In this case, entire domain is initialized. Variables is entered with two group. One group contains static pressure, static temperature, and velocity, other one contains static pressure, static density, and velocity. The first group is selected because of test case.

Table 2.1: Initial conditions for probe. [7]

Static Pressure [Pa]		148.88
Static Temperature [K]		724
Velocity [m/s]	x	3257
	y	0
	z	0
Mass Fractions	C	0
	C_2	0
	CO	0.279
	O	0.01
	O_2	0.149
	CO_2	0.562

2.2.2.4 Initial boundary conditions

There are four boundary types. These are inlet, outlet, symmetry, and wall. Inlet boundary condition contains the initial conditions.

For inlet boundary condition, supersonic inflow-all conditions prescribed (temperature) is selected. This condition is using for Mach over than one. Its values are selected from initial conditions. All value of Table 2.1 is valid for inlet boundary condition.

For outlet boundary condition, centroidal extrapolation-no condition prescribed condition is selected because after body interaction flow field cannot be predicted. There is no need to enter any value.

For symmetry condition, basic symmetry condition is selected. There is no need to enter any value. Its values are determined by domain.

For wall condition, there are many different selections. Wall type is viscous (no-slip). The wall heat transfer's condition is isothermal-constant temperature. The wall temperature is 300 K. The wall integration way is solve to wall. Wall is stationary-with respect to the mesh motion. It is super-catalytic wall. The wall species are zero. Next, the wall temperature relaxation is starting from step number is thirty and ending step number is two hundred thirty.

2.2.2.5 Time Integration and Spatial Discretization

The time step size is $5e^{-8}$. Simulation is transient and integration type is implicit. For probe, 14000 steps is run. For Pathfinder entry vehicle, 60000 steps are run. Pathfinder entry vehicle's domain is bigger than probe's domain. Therefore, Pathfinder's step number is bigger than probe's step numbers. Order of inviscid discretization is second order. Dimensionality of polynomial is 2-D-Axisymetric. 2-D-Axisymetric provides solving 3D cases by using 2D domain. It is solving 2-D by adding 3-D effects. However, the geometry and flow must be symmetric around an axis. A flow that has an angle of attack cannot be solved. In these cases, two domains and flows are symmetric.

2.3 Flow at Martian Entry Conditions around Pathfinder Entry Vehicle

Pathfinder entry vehicle's geometry is selected for training case. This same geometry also was used for Mars Exploration Rover and Phoenix Mars Missions. The entry vehicle basic geometry's picture is shown in Figure 2.4.

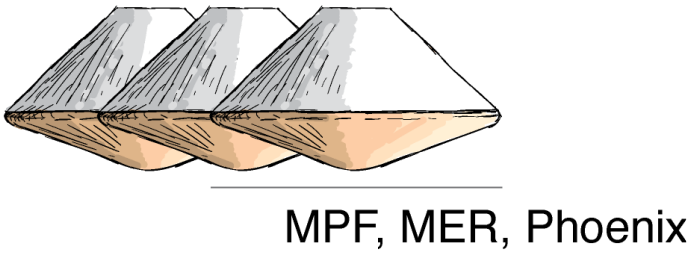

Figure 2.4: MPF, MER and Phoenix entry vehicle basic pictures. [5]

2.3.1 Mesh generation

The pathfinder geometry was created via CATIA V5 R20 program. This program is generally used for creating solid 3D design for machine parts etc. In this study, it is used for creating 2D drawing for creating boundaries of Pathfinder spacecraft's flow field. The model of Pathfinder is shown in Figure 2.5. Next, dimensions of spacecraft and domain is shown in Figure 2.6.

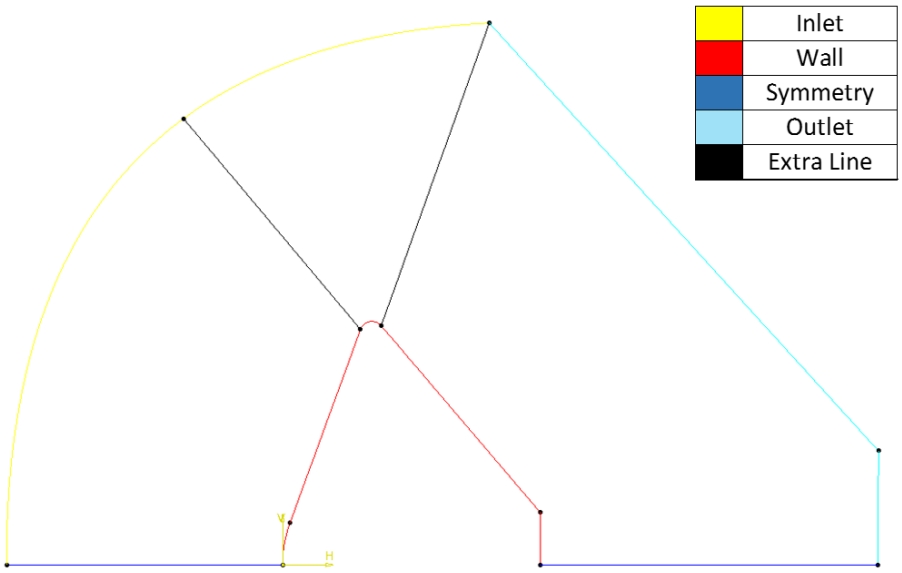

Figure 2.5: 2D Geometry model created via CATIA.

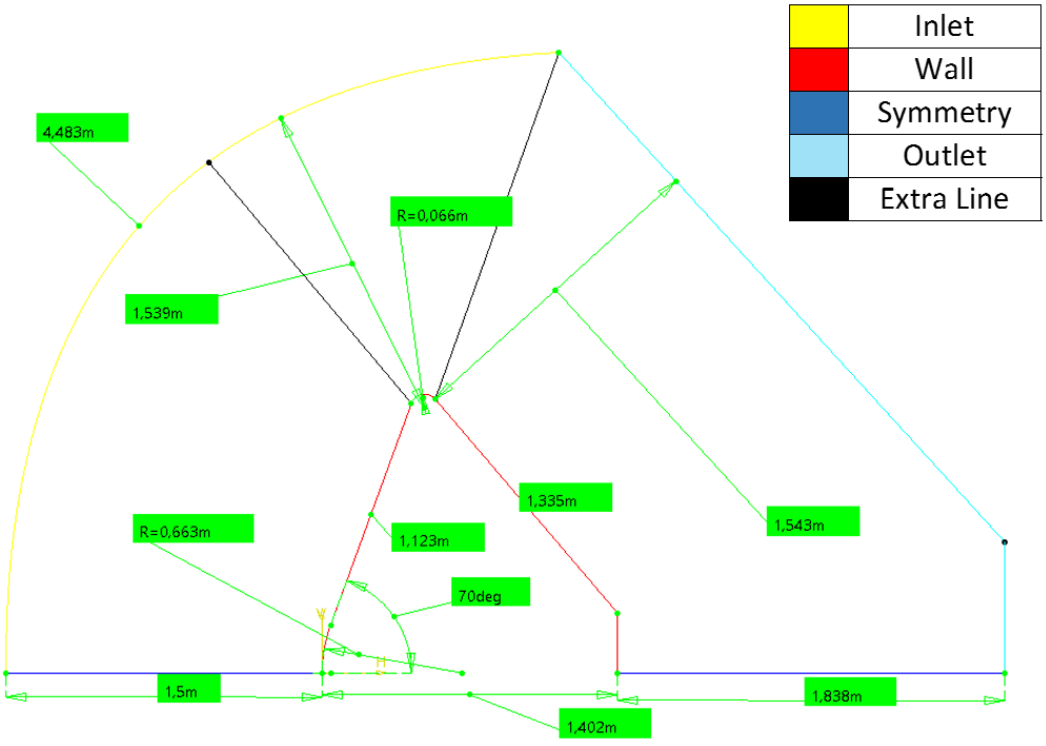

Figure 2.6: Dimensions of domain and geometry.

Mesh for the geometry is generated via Pointwise program. This program is so useful for 2D mesh creation. The mesh is structured. CFD++ is able to solve structured and unstructured meshes; however, because of clearly displaying shocks, structured mesh is preferred. There are 159200 quadrilateral cells in computational domain. First

element distance from nose of wall is 10^{-6} m. Skewness of equiangle is maximum 0.3545. In Figure 2.7, the mesh of the Pathfinder entry vehicle is shown. Skewness of equiangle is important for solution. It needs to be under 0.8. The skewness of equiangle values are shown in Figure 2.8. If results of flow would be accurate, area ratio needs to be small. Area ratios value are shown in Figure 2.9.

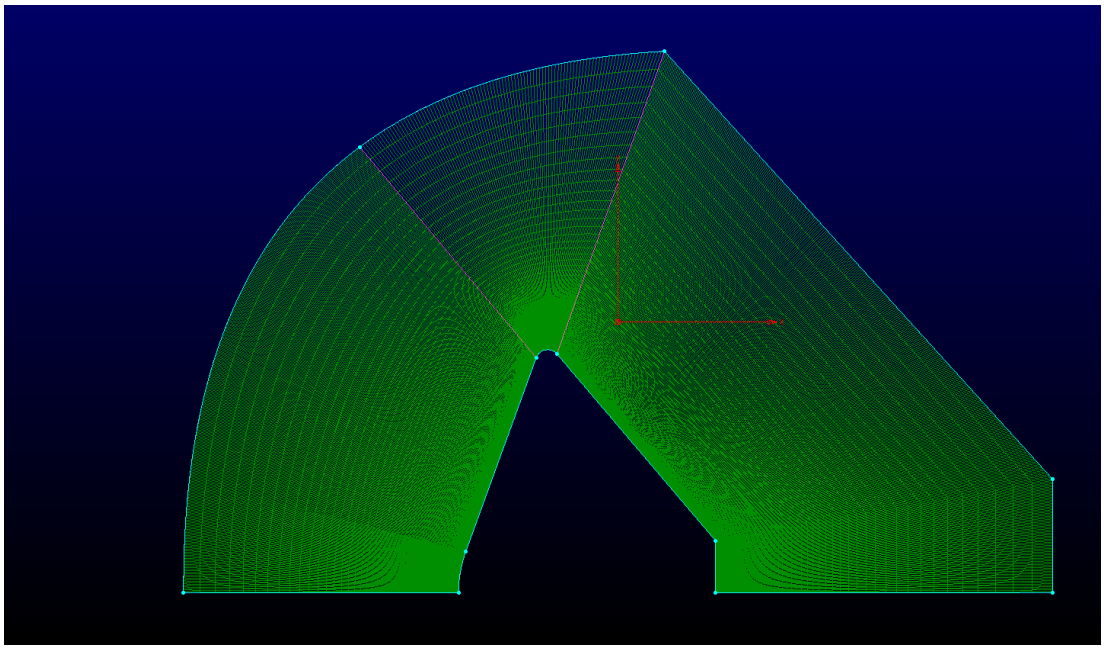

Figure 2.7: Pathfinder entry vehicle mesh model.

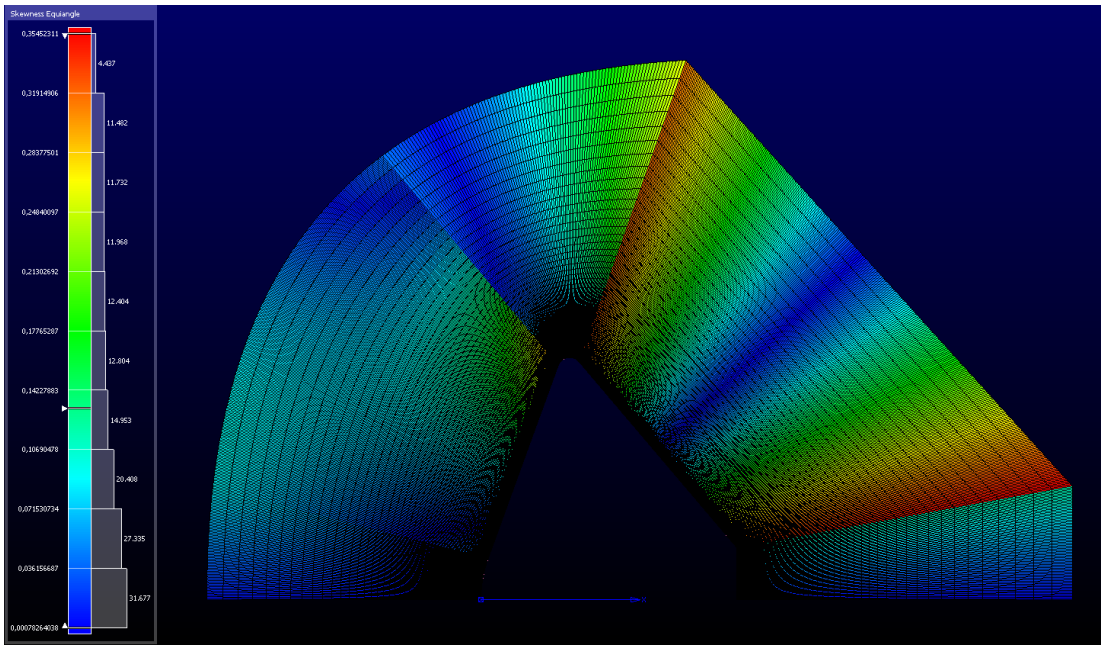

Figure 2.8: The mesh model's skewness equiangle.

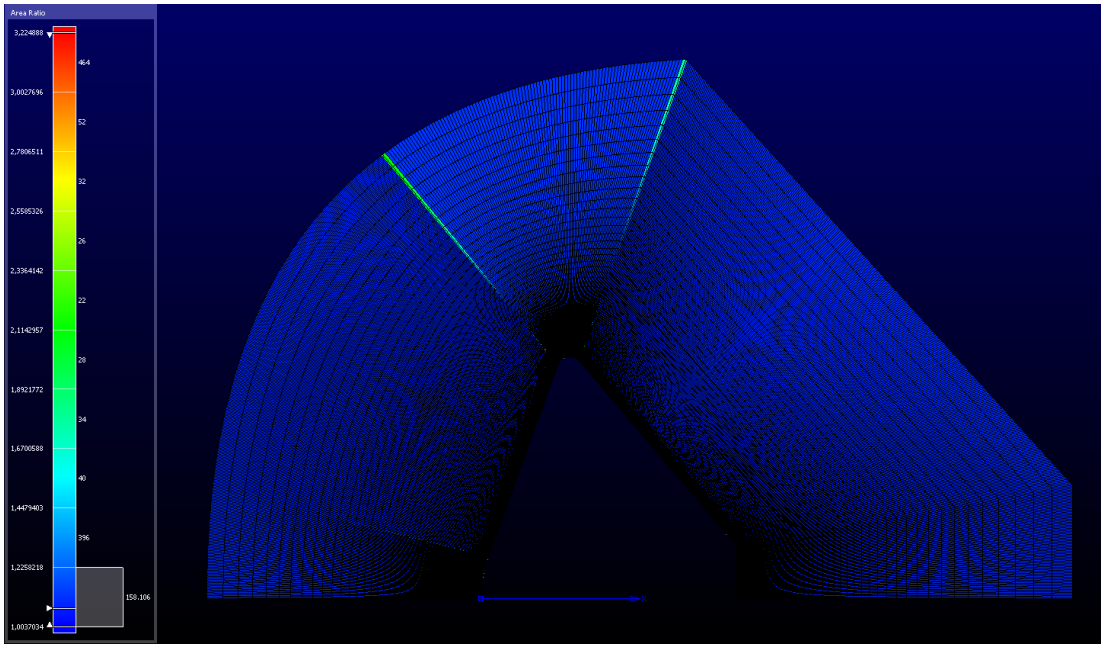

Figure 2.9: The mesh model's area ratio.

The most important point is that first node’s distance from wall for simulating flow near wall. Wall spacing is shown in Figure 2.10.

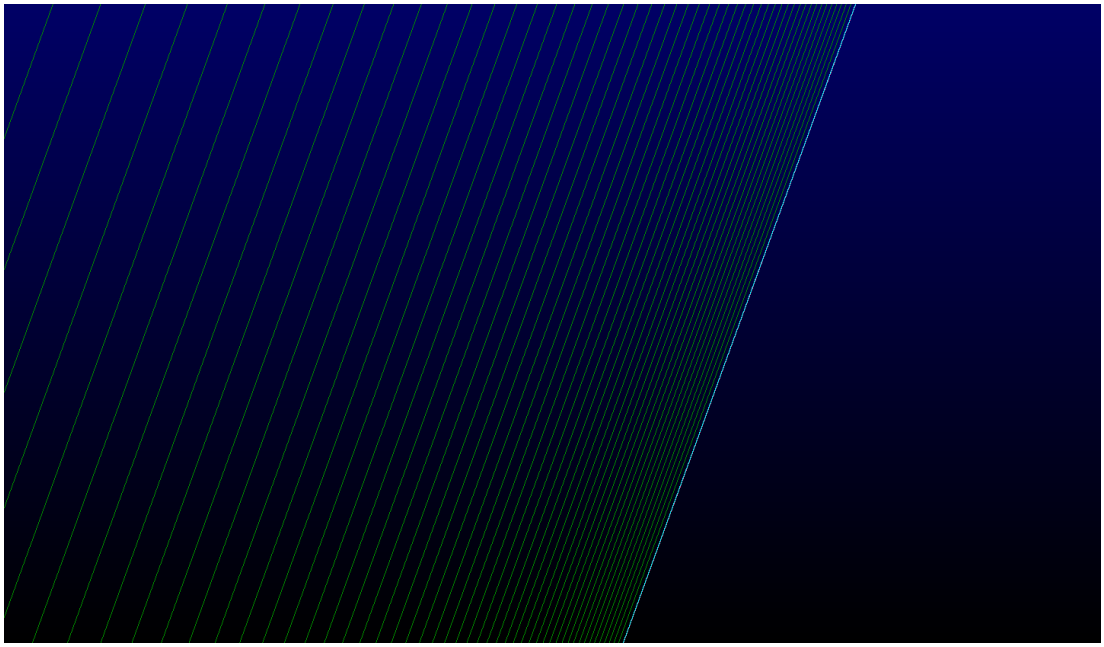

Figure 2.10: The mesh model's wall spacing.

Boundary conditions are set by using Pointwise. After that, boundary conditions occurred on CFD++.

2.3.2 CFD modelling

This modelling is same as the probe case. Same conditions are preferred for using and comparing between two cases. Differences of cases are only geometry. The probe geometry results are proofed with papers and comparing. Therefore, the Pathfinder entry vehicle's case can be assumed that results are valid under same conditions. The initial conditions are shown in Table 2.2.

Table 2.2: Initial conditions for Pathfinder entry vehicle. [7]

Static Pressure [Pa]		148.88
Static Temperature [K]		724
Velocity [m/s]	x	3257
	y	0
	z	0
Mass Fractions	C	0
	C_2	0
	CO	0.279
	O	0.01
	O_2	0.149
	CO_2	0.562

3. RESULTS AND DISCUSSION

3.1 Results of Cylindrical Probe

Computational results for Martian entry of a cylindrical probe are shown in this Section. Maximum y+ value and cell Reynolds number are 0.66929, 0.44815, respectively. Maximum heat transfer rate is calculated 1.365e^{6} W/m^{2}. Pressure distribution is shown in Figure 3.1 for probe. The maximum value is 9019.03 Pa.

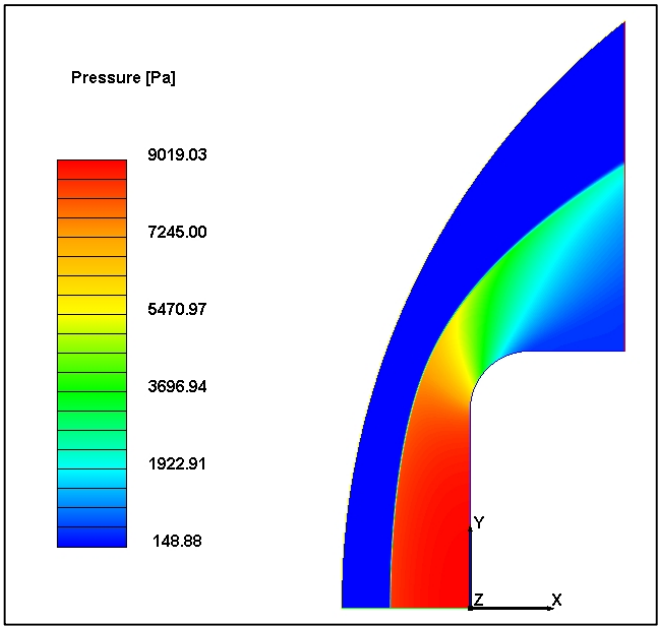

Figure 3.1: Pressure distribution around probe's flow field.

Variation of temperature around the probe is shown in Figure 3.2 below. The maximum temperature value is 4643.88 K. It is larger than the Pathfinder's maximum because of angle of cone.

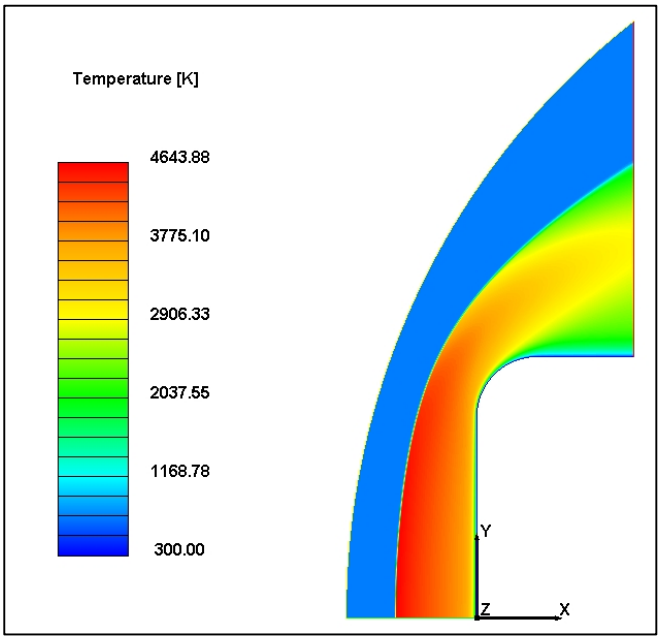

Figure 3.2: Temperature distribution around probe's flow field.

Behind the bow shock, local temperatures of the two cases are different because of the relatively simple geometry of the probe. As can be seen from the figures, there is an additional shock between the bow shock and the geometry for the probe case.

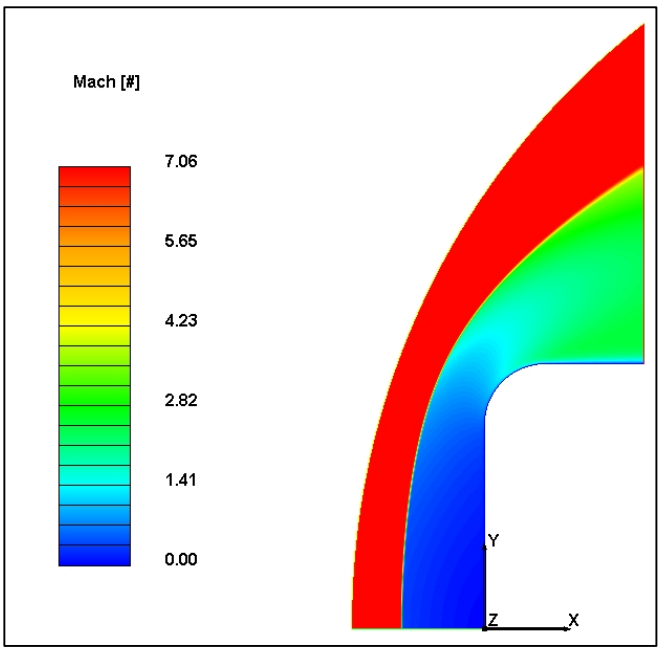

Figure 3.3: Mach results for probe's flow field.

The probe’s mass fraction distributions of molecules and atoms are shown in following figures.

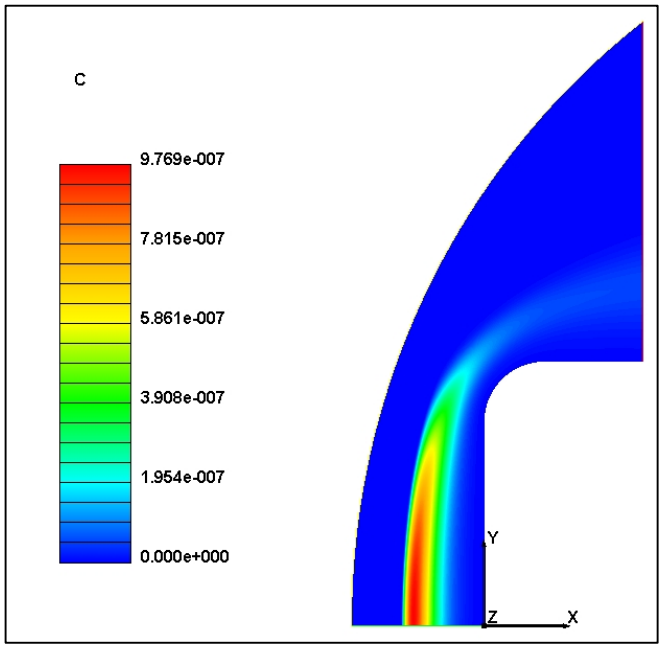

Figure 3.4: C Atoms distribution around probe's flow field.

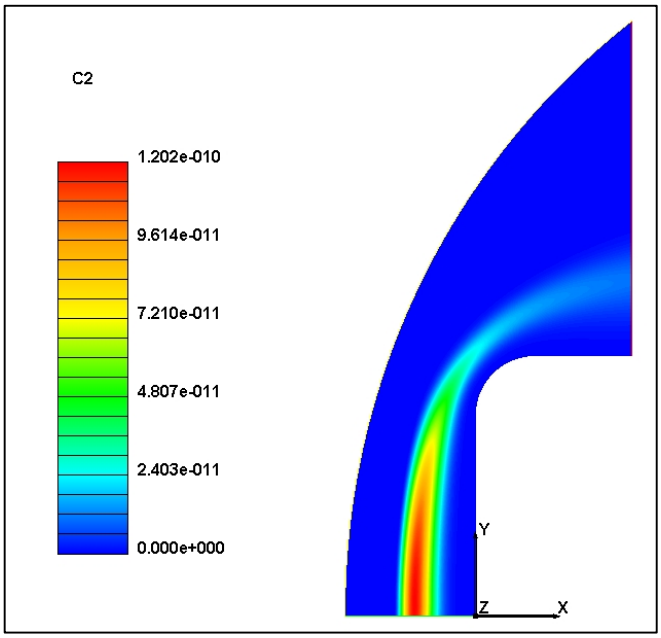

Figure 3.5: C_2 Molecules distribution around probe's flow field.

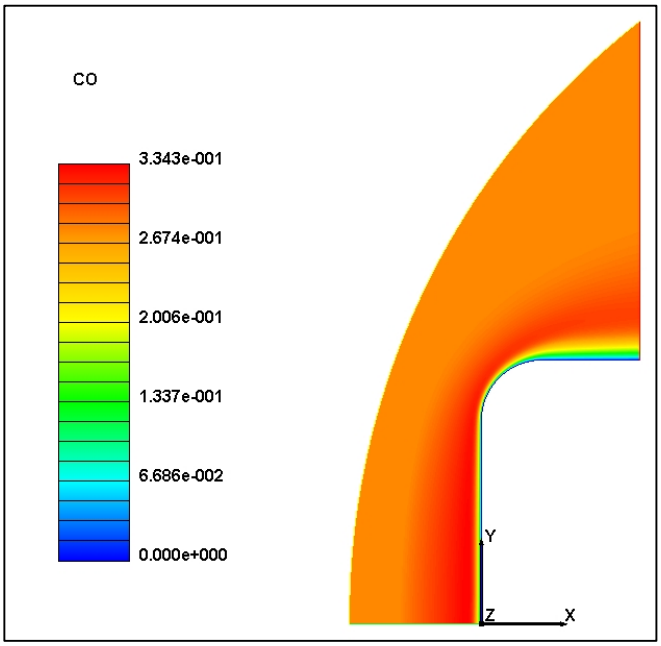

Figure 3.6: CO Molecule distribution around probe's flow field.

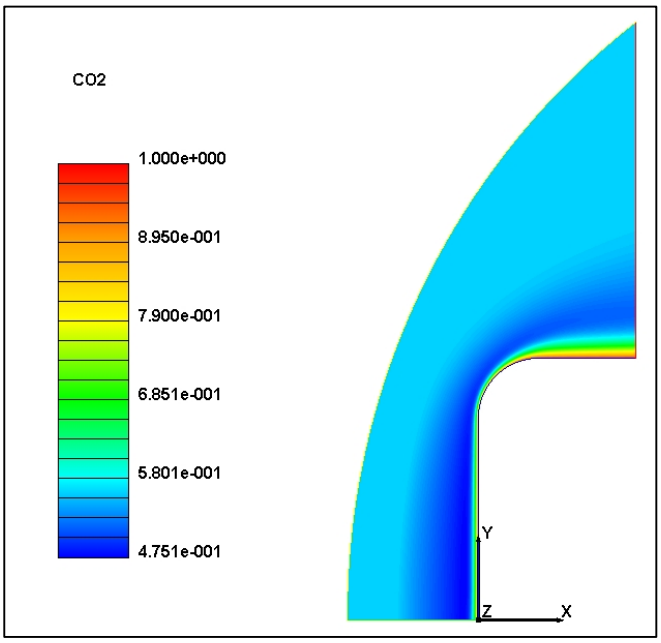

Figure 3.7: CO_2 Molecules distribution around probe's flow field.

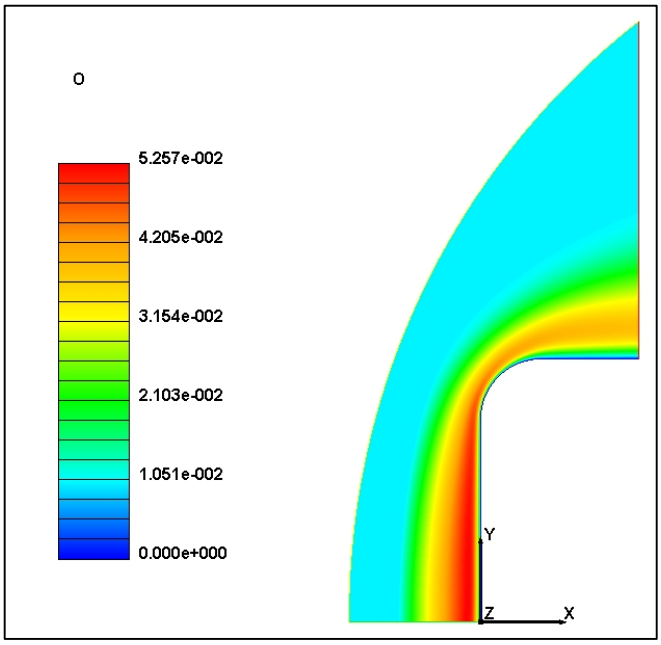

Figure 3.8: O Atoms distribution around probe's flow field.

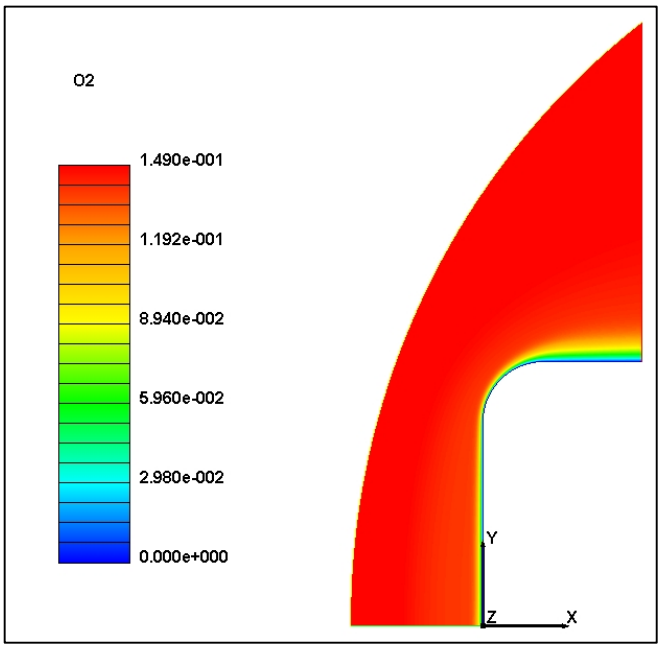

Figure 3.9: O_2 Molecules distribution around probe's flow field.

Distribution of pressure and heat flux on the probe surface are also compared with DLR test case data. A comparison graphic is shown in Figure 3.10.

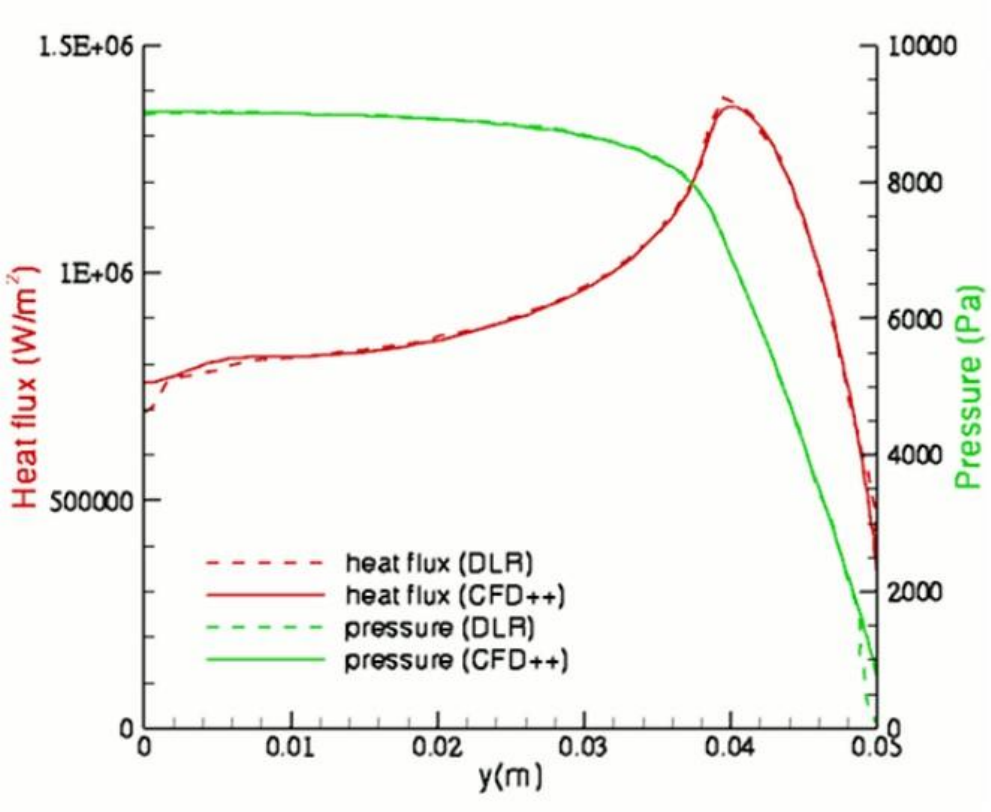

Figure 3.10: The probe case results comparing with DLR results. [8]

3.2 Results of Pathfinder Entry Vehicle

Results of the Pathfinder entry vehicle's case are shown in following the figures of Section 3.2. The maximum of y+ value is calculated 0.0751. Maximum of cell Reynolds number is computed 0.005641. Maximum heat transfer rate is equal to $7.136e^6$ W/m^2. Pressure variation is shown in Figure 3.11 for Pathfinder entry vehicle. Its maximum value is 9049.27 Pa. The difference with the probe is 30.24 Pa.

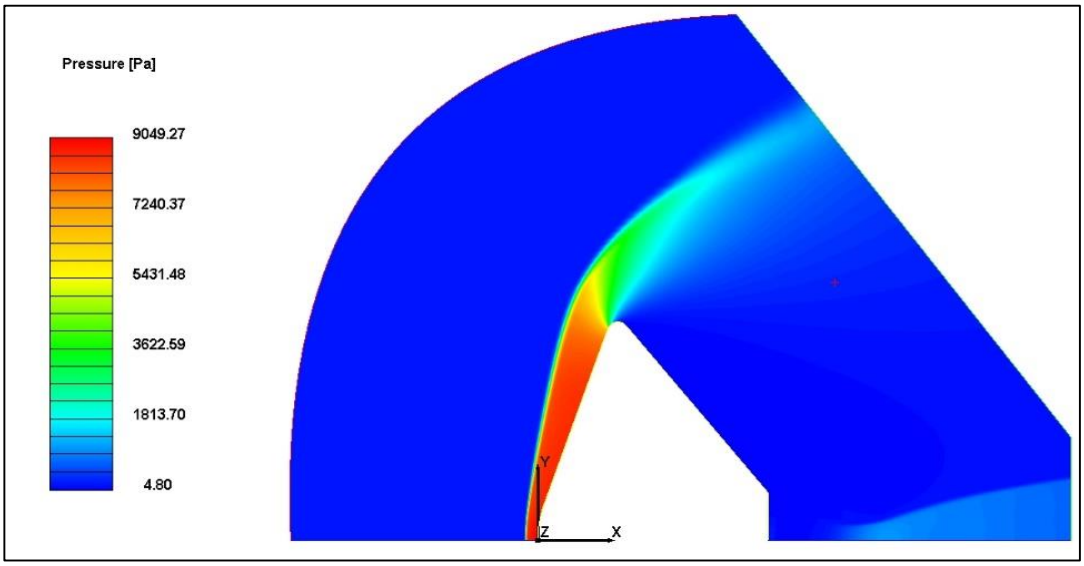

Figure 3.11: Pressure distribution around Pathfinder entry vehicle's flow field.

Temperature variation around the Pathfinder is shown in Figure 3.12 below. The maximum temperature value is 4365.43 K, which is smaller than the cylindrical probe's maximum.

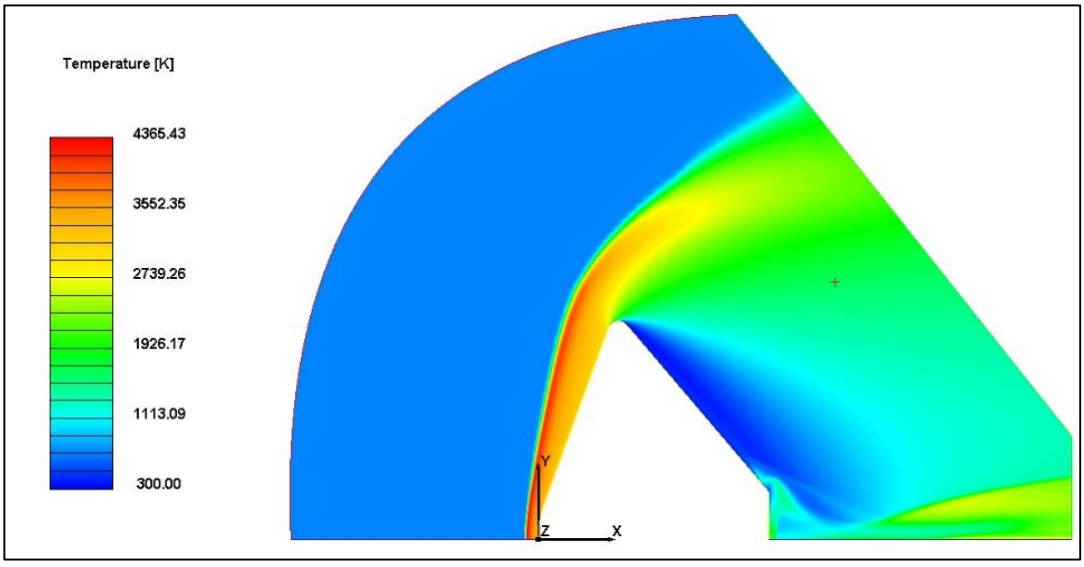

Figure 3.12: Temperature distribution around Pathfinder entry vehicle's flow field.

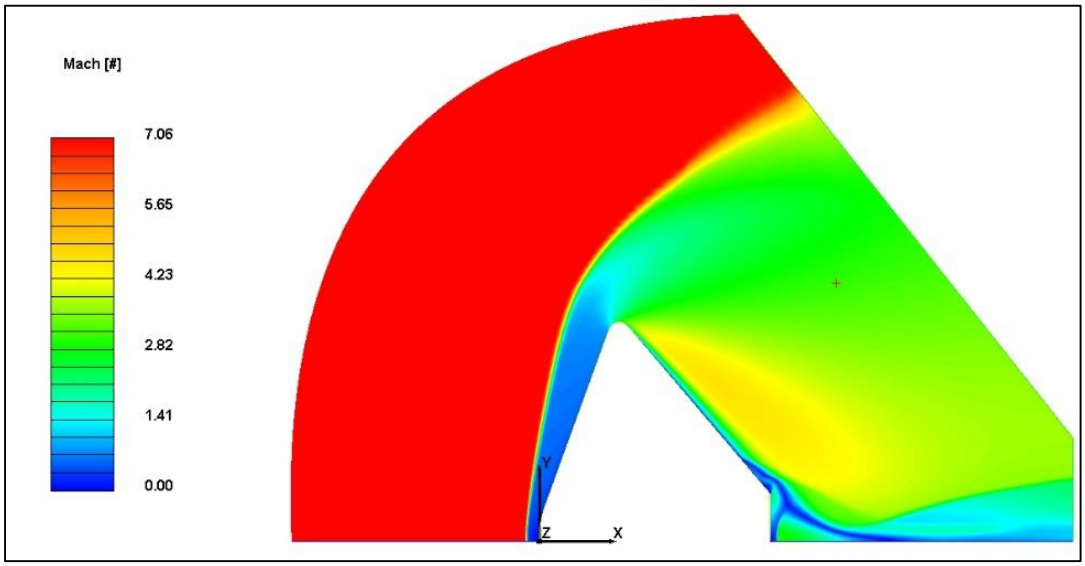

Figure 3.13: Mach results for Pathfinder entry vehicle's flow field.

All atoms and molecules mass fractions are shown in following figures.

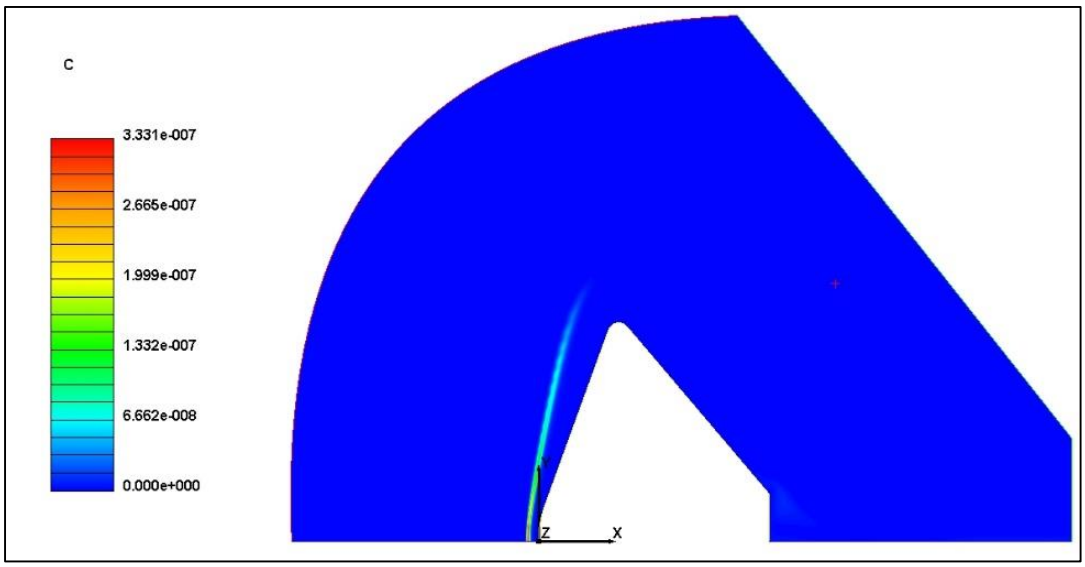

Figure 3.14: C Atoms distribution around Pathfinder entry vehicle's flow field.

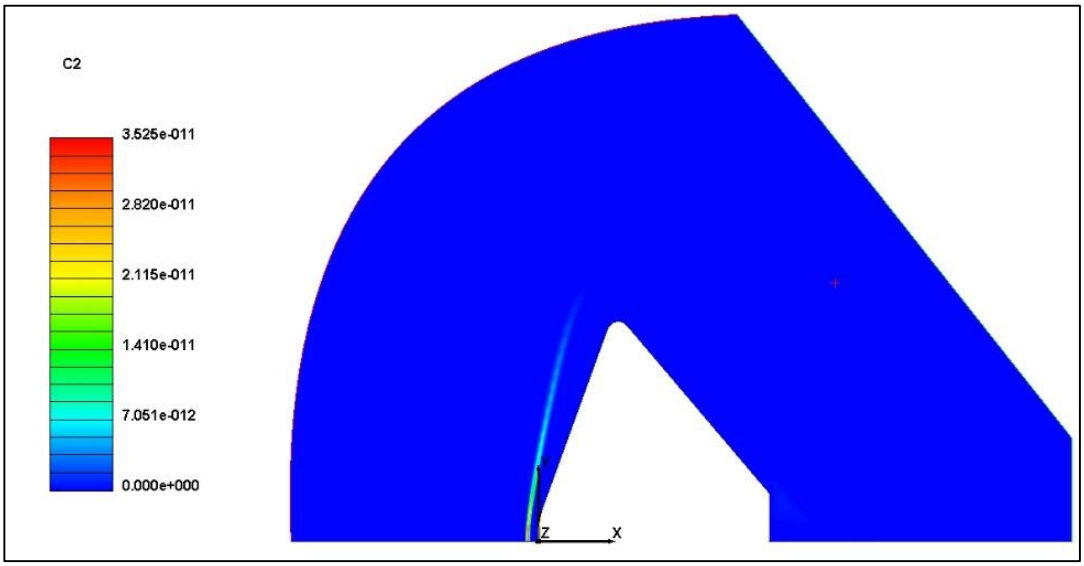

Figure 3.15: C_2 Molecules distribution around Pathfinder entry vehicle's flow field.

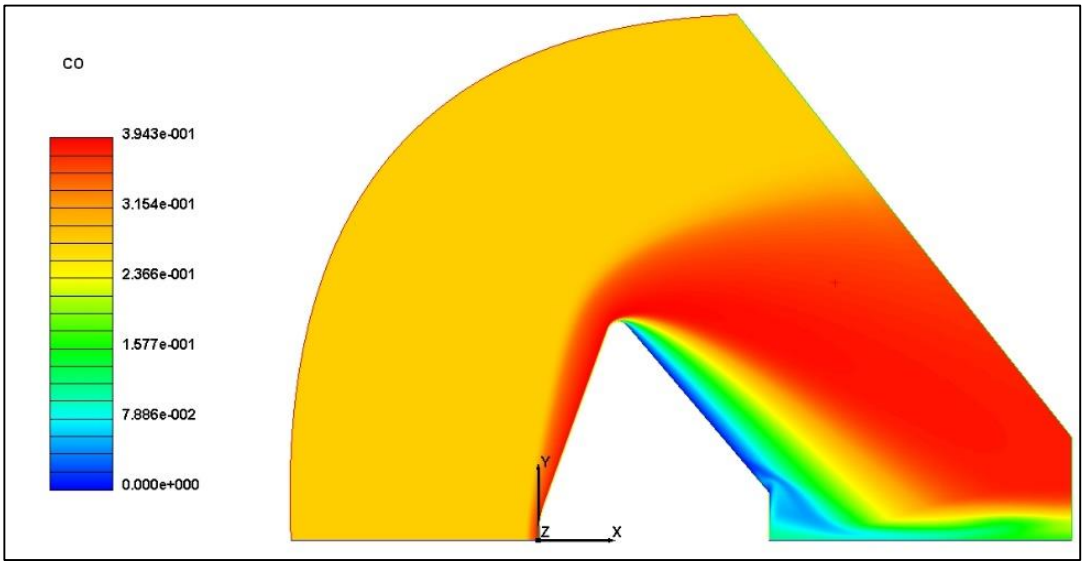

Figure 3.16: CO Molecules distribution around Pathfinder entry vehicle's flow filed.

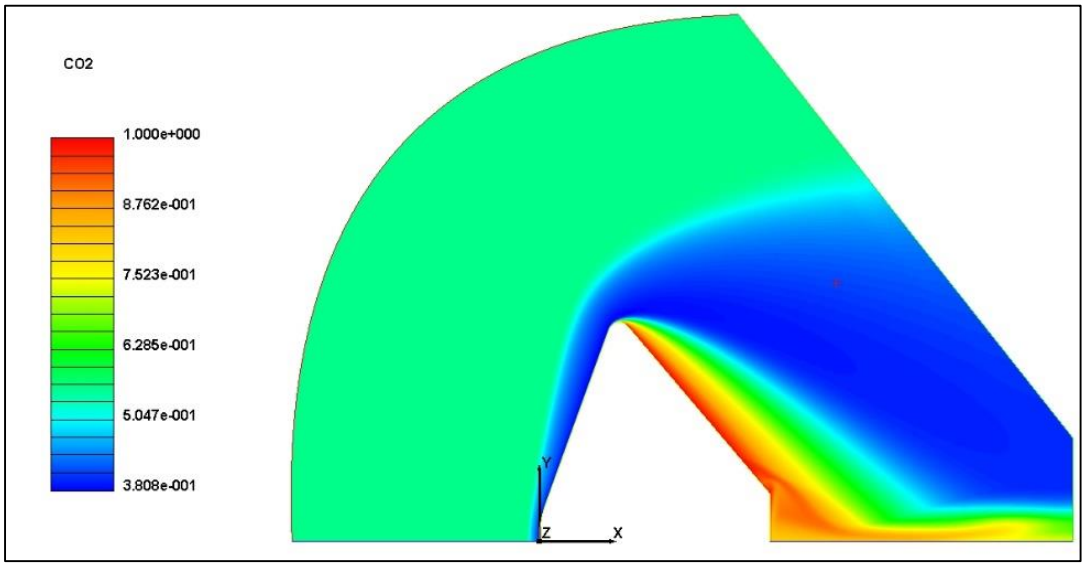

Figure 3.17: CO_2 Molecules distribution around Pathfinder entry vehicle's flow field.

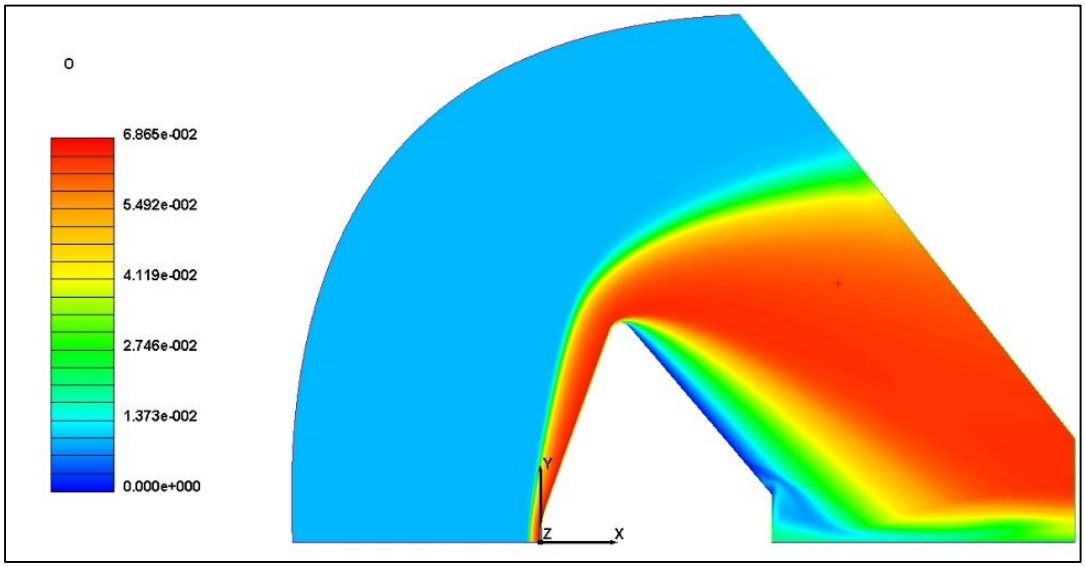

Figure 3.18: O Atoms distribution around Pathfinder entry vehicle's flowfield.

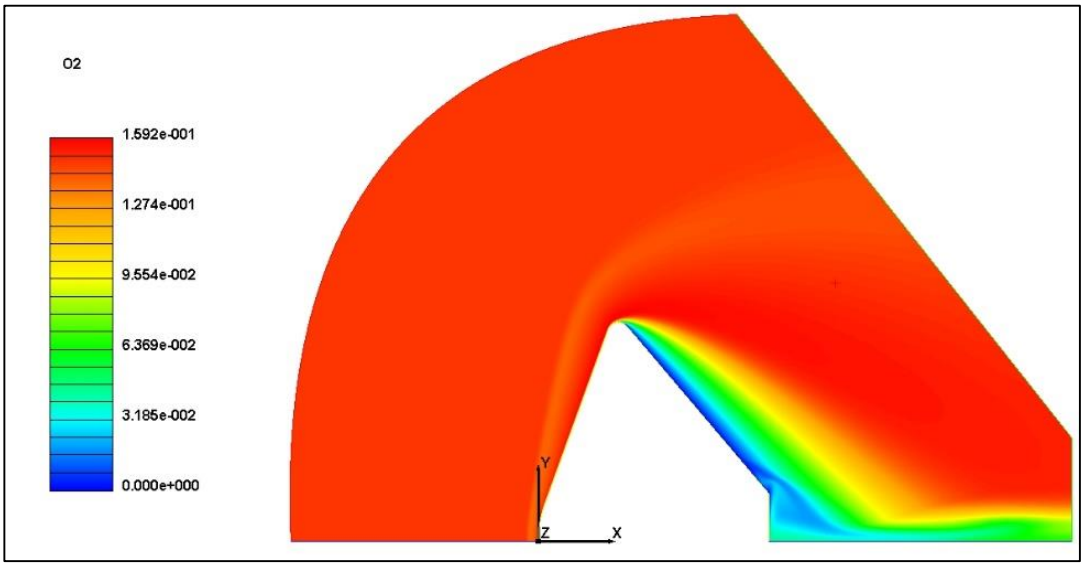

Figure 3.19: O_2 Molecules distribution around Pathfinder entry vehicle's flow field.

4. CONCLUSION

According to the results obtained for the pathfinder and the comparison of the DLR's results with CFD++ results, the solutions are reasonably accurate. In order to test the solver, an additional geometry, a cylindrical probe is modelled and analyzed. All the results are shown in Chapter 3.

This study shows that there is no big difference in the maximum pressure value of the two cases. The probe's maximum pressure is 9019.03 Pa and Pathfinder's maximum pressure is 9049.27 Pa. The difference is only 30.24 Pa. Maximum temperature takes place immediately after the bow shocks, which are equal to 4365.43 K and 4643.88 K for Pathfinder and Probe's cases, respectively. The temperature difference is 278.45 K. This results show that the blunt body, which has an angle lower than the 90^{o} with respect to the flow direction is more efficient in terms of ejecting the hot gas from vehicle's front. In addition to the pressure and temperature variations, distributions of atoms and molecules are examined.

As a result, this thesis project gives a chance to understand basics of an entry vehicle geometry and the challenges of CFD modelling of an entry vehicle.

REFERENCES

[1] "NASA," [Online]. Available: http://mars.jpl.nasa.gov/MPF/mpf/fact_sheet.html. [Accessed 15 AUGUST 2014].

[2] "Federal Aviation Administration," [Online]. Available: https://www.faa.gov/other_visit/aviation_industry/designees_delegations/designee_types/ame/media/Section%20III.4.1.7%20Returning%20from%20Space.pdf. [Accessed 15 AUGUST 2014].

[3] "NASA," [Online]. Available: http://www.hq.nasa.gov/pao/History/SP-4209/ch3-4.htm. [Accessed 15 AUGUST 2014].

[4] [Online]. Available: http://nassp.sourceforge.net/wiki/Entry_Monitoring_System. [Accessed 15 AUGUST 2014].

[5] Karl Edquist, Mark Schoenenberger, and Mike Wright, "Solar System Exploration," 26 June 2013. [Online]. Available: https://solarsystem.nasa.gov/docs/Day%201_05_IPPW-10%20EDL%20Short%20Course%20Aero%20No%20Backup.pdf.

[6] Frank J. REGAN, Satya M. ANANDAKRISHNAN, Dynamics of Atmospheric Re-Entry, Maryland: Silver Spring, 1993, pp. 310, 328.

[7] Jan Martinez Schramm, "SACOMAR," 21 Febuary 2012. [Online]. Available: http://www.dlr.de/as/en/Portaldata/5/Resources/dokumente/projekte/sacomar/S

ACOMAR_D5_2_DLR_Experimental_Study_HEG.pdf. [Accessed 18 August 2014].

[8] M. FERTIG, "SACOMAR," 10 Febuary 2012. [Online]. Available: http://www.dlr.de/as/en/Portaldata/5/Resources/dokumente/projekte/sacomar/SACOMAR_D6_3_DLR_Gas_Phase_Chemistry.pdf. [Accessed 18 August 2014].

APPENDICES

APPENDIX A.1: Reactions

APPENDIX A.2: Inputs of reactions

APPENDIX A.1

Table A.1: Reactions and its components. [8]

Number of Reaction	Reactants		Products
1	1.0 CO_2 + 1.0 CO_2	<->	1.0 CO + 1.0 O + 1.0 CO_2
2	1.0 CO_2 + 1.0 CO	<->	1.0 CO + 1.0 O + 1.0 CO
3	1.0 CO_2 + 1.0 O_2	<->	1.0 CO + 1.0 O + 1.0 O_2
4	1.0 CO_2 + 1.0 C	<->	1.0 CO + 1.0 O + 1.0 C
5	1.0 CO_2 + 1.0 O	<->	1.0 CO + 1.0 O + 1.0 O
6	1.0 CO + 1.0 CO_2	<->	1.0 C + 1.0 O + 1.0 CO_2
7	1.0 CO + 1.0 CO	<->	1.0 C + 1.0 O + 1.0 CO
8	1.0 CO + 1.0 O_2	<->	1.0 C + 1.0 O + 1.0 O_2
9	1.0 CO + 1.0 C	<->	1.0 C + 1.0 O + 1.0 C
10	1.0 CO + 1.0 O	<->	1.0 C + 1.0 O + 1.0 O
11	1.0 O_2 + 1.0 CO_2	<->	2.0 O + 1.0 CO_2
12	1.0 O_2 + 1.0 CO	<->	2.0 O + 1.0 CO
13	1.0 O_2 + 1.0 O_2	<->	2.0 O + 1.0 O_2
14	1.0 O_2 + 1.0 C	<->	2.0 O + 1.0 C
15	1.0 O_2 + 1.0 O	<->	2.0 O + 1.0 O
16	1.0 CO + 1.0 O	<->	1.0 C + 1.0 O_2
17	1.0 CO_2 + 1.0 O	<->	1.0 CO + 1.0 O_2
18	1.0 CO_2 + 1.0 C_2	<->	1.0 CO + 1.0 O + 1.0 C_2
19	1.0 C_2 + 1.0 CO_2	<->	1.0 C + 1.0 C + 1.0 CO_2
20	1.0 C_2 + 1.0 CO	<->	1.0 C + 1.0 C + 1.0 CO
21	1.0 C_2 + 1.0 C_2	<->	1.0 C + 1.0 C + 1.0 C_2
22	1.0 C_2 + 1.0 O_2	<->	1.0 C + 1.0 C + 1.0 O_2
23	1.0 C_2 + 1.0 C	<->	1.0 C + 1.0 C + 1.0 C
24	1.0 C_2 + 1.0 O	<->	1.0 C + 1.0 C + 1.0 O
25	1.0 CO + 1.0 C_2	<->	1.0 C + 1.0 O + 1.0 C_2
26	1.0 O_2 + 1.0 C_2	<->	1.0 O + 1.0 O + 1.0 C_2
27	1.0 CO + 1.0 C	<->	1.0 C_2 + 1.0 O

APPENDIX A.2

Table A.2: Reactions inputs. [8]

Number of Reaction	Frequency Factor [m³/mole/s]	Temperature Exponent [-]	Activation Energy [Nm/kmol]
1	$6.9e^{18}$	-1.5	$5.26e^{8}$
2	$6.9e^{18}$	-1.5	$5.26e^{8}$
3	$6.9e^{18}$	-1.5	$5.26e^{8}$
4	$1.4e^{19}$	-1.5	$5.26e^{8}$
5	$1.4e^{19}$	-1.5	$5.26e^{8}$
6	$2.3e^{17}$	-1.0	$1.07e^{9}$
7	$2.3e^{17}$	-1.0	$1.07e^{9}$
8	$2.3e^{17}$	-1.0	$1.07e^{9}$
9	$3.4e^{17}$	-1.0	$1.07e^{9}$
10	$3.4e^{17}$	-1.0	$1.07e^{9}$
11	$2.0e^{18}$	-1.5	$4.97e^{8}$
12	$2.0e^{18}$	-1.5	$4.97e^{8}$
13	$2.0e^{18}$	-1.5	$4.97e^{8}$
14	$1.0e^{19}$	-1.5	$4.97e^{8}$
15	$1.0e^{19}$	-1.5	$4.97e^{8}$
16	$3.9e^{10}$	-0.18	$5.75e^{8}$
17	$2.1e^{10}$	0	$2.31e^{8}$
18	$6.9e^{18}$	-1.5	$5.26e^{8}$
19	$1.5e^{13}$	0	$5.95e^{8}$
20	$1.5e^{13}$	0	$5.95e^{8}$
21	$1.5e^{13}$	0	$5.95e^{8}$
22	$1.5e^{13}$	0	$5.95e^{8}$
23	$1.5e^{13}$	0	$5.95e^{8}$
24	$1.5e^{13}$	0	$5.95e^{8}$
25	$2.3e^{17}$	-1.0	$1.07e^{9}$
26	$2.0e^{18}$	-1.5	$4.97e^{8}$
27	$2.0e^{14}$	-1.0	$4.82e^{8}$